remote sensing

MDPI

Article

Reliability of GPM IMERG Satellite Precipitation Data for Modelling Flash Flood Events in Selected Watersheds in the UAE

Mohamed A. Hamouda [1,2,*], Gilbert Hinge [3], Henok S. Yemane [1], Hasan Al Mosteka [1], Mohammed Makki [1] and Mohamed M. Mohamed [1,2]

[1] Department of Civil and Environmental Engineering, United Arab Emirates University, Al Ain P.O. Box 15551, United Arab Emirates; 201850214@uaeu.ac.ae (H.S.Y.); 202007808@uaeu.ac.ae (H.A.M.); 202050901@uaeu.ac.ae (M.M.); m.mohamed@uaeu.ac.ae (M.M.M.)
[2] National Water and Energy Center, United Arab Emirates University, Al Ain P.O. Box 15551, United Arab Emirates
[3] Department of Civil Engineering, National Institute of Technology Durgapur, Durgapur 713209, India; gilbert.hinge@ce.nitdgp.ac.in
* Correspondence: m.hamouda@uaeu.ac.ae

Abstract: Arid regions are prone to unprecedented extreme rainfall events that often result in severe flash floods. Using near-real-time precipitation data in hydrological modelling can aid in flood preparedness. This study analyzed rainfall data obtained from Integrated Multi-satellite Retrievals for Global Precipitation Measurement (IMERG V. 06) since 2001 to highlight recent trends of extreme rainfall indices for three selected watersheds in the UAE. Additionally, to validate the trends, the present study incorporated CHIRPS (Climate Hazards Group InfraRed Precipitation with Station data) into the analysis. Furthermore, for the first time, this study assessed the performance of the three products of IMERG in modelling flash flood events in the selected watersheds of UAE. A physical-based, fully distributed model was used to simulate the heaviest storm event. Also, a sensitivity analysis of the model's output to variations in the input parameters was conducted using the one-factor-at-a-time method. The result of the trend analysis indicated that IMERG and CHIRPS show similar trends in both datasets, indicating agreement and reliability in their observations. However, there are a few instances where IMERG and CHIRPS show slight discrepancies in the nature of the trend. In general, the trend analysis results indicated an increasing trend of total precipitation (mm) and consecutive wet days, which suggests a rise in the risk of flash floods. The simulation of the flash flood event showed that the IMERG final product outperformed the other two products, closely matching the model output of the gauge rainfall data with mean absolute error (MAE) of 1.5, 2.37, and 0.5 for Wadi Ham, Wadi Taween, and Wadi Maidaq, respectively. The model's performance was positively correlated with the size of the watershed. The sensitivity analysis results demonstrated that the model's output was most sensitive to infiltration parameters. The study's outcomes provide a good opportunity to improve near-real-time impact evaluation of flash flood events in the watersheds of the UAE.

Keywords: extreme rainfall; flash floods; GSSHA; GPM IMERG; sensitivity analysis

Citation: Hamouda, M.A.; Hinge, G.; Yemane, H.S.; Al Mosteka, H.; Makki, M.; Mohamed, M.M. Reliability of GPM IMERG Satellite Precipitation Data for Modelling Flash Flood Events in Selected Watersheds in the UAE. *Remote Sens.* **2023**, *15*, 3991. https://doi.org/10.3390/rs15163991

Academic Editors: Alfred J. Kalyanapu, Venkata Reddy Keesara and Md Nowfel Mahmud Bhuyian

Received: 24 June 2023
Revised: 25 July 2023
Accepted: 28 July 2023
Published: 11 August 2023

1. Introduction

Flash floods, commonly triggered by rainfall of short duration and high intensity, can constitute a hazardous natural disaster, causing severe damage to the built environment [1]. In recent years, flash floods have drastically increased due to climate change and exacerbating urbanization [2]. For instance, in July 2021, several European countries, including Germany, Belgium, Italy, Austria, and Romania, were affected by severe flash floods causing loss of life and property [3]. Similarly, many flash flood incidents were

reported in India, China, Turkey, and several other arid and semi-arid countries [4–6]. In the United Arab Emirates, several flash floods were reported in many cities, such as Al Ain, Fujairah, Al Qurayah, and the Sharm [5]. Thus, there is a need to monitor, model, and forecast flash floods to increase preparedness and resilience, particularly in arid countries.

Modelling and predicting flash floods often rely on hydrological modelling tools [2]. Hydrological models are simplifications of reality and are designed to simulate the key hydrological processes and interactions within a watershed [2,7]. The accuracy of the model's outputs depends heavily on the quality and representativeness of the input data. The main inputs required for sophisticated hydrological models include rainfall data, topographical data, soil data, and land use and land cover (LULC) [7]. Nevertheless, rainfall data are particularly challenging for ungauged or poorly gauged watersheds. In recent years, researchers have resorted to satellite precipitation products (SPPs) as accessible data sources with acceptable accuracy [8,9]. SPPs provide global rainfall data at high spatial and temporal resolutions. SPPs have been applied to numerous hydrological models to model extreme rainfall events [10–12].

One of the most promising SPPs is the Integrated Multi-Satellite Retrievals for the Global Precipitation Mission (IMERG). The major advancement of IMERG over other SPPs is its ability to detect light rains and different types of precipitation, including snowfall and rainfall [13]. This is possible because of its two advanced instruments, namely the Dual-frequency Precipitation Radar (DPR) and microwave radiometer called GPM Microwave Imager (GMI), as well as advancements in precipitation retrieval algorithms, calibration techniques, and the incorporation of morphing techniques [14]. Additionally, compared to other SPPs, IMERG has a high spatial resolution ($0.1^\circ \times 0.1^\circ$) and a half-hourly temporal resolution [14]. Three types of IMERG Products are available: IMERG Early Run, IMERG Late Run, and IMERG Final Run. The latency periods of IMERG Early and Late products are approximately 6 to 18 h. The IMERG Final product is adjusted based on gauge data available at the Global Precipitation Climatology Centre (GPCC), and its latency period is approximately three months after the observation day. Many studies have compared IMERG and other SPPs and have reported that GPM IMERG significantly improves the performance of hydrological model outputs compared to other SPPs [9,15–17]. Few studies have used ground observations not included in GPCC to further evaluate the performance of IMERG in arid regions [14,18,19]; their results demonstrated a good agreement between IMERG and ground observations to accurately capture the precipitation patterns, both in terms of frequency and intensity

In addition to the rainfall variability, the spatiotemporal variations of other hydrological model inputs, such as topography, LULC, and soil types, significantly affect a model's performance [20]. Furthermore, the scale of these factors plays a critical role in accurately representing and simulating hydrological processes, encompassing the spatial extent and resolution at which these factors are considered in the hydrological model. Gridded fully distributed models can better represent the modeled watershed than lumped and semi-distributed models. The Gridded Surface Subsurface Hydrologic Analysis (GSSHA) model is a gridded fully distributed model that has been used for flash flood modelling [20]. Many studies have used SPPs as an input into the GSSHA models and reported that GSSHA produces reliable results [21–23]. However, GSSHA and similar gridded fully distributed models require numerous input data. Nevertheless, input parameters do not equally influence the reliability and accuracy of the model's output [23]. The relative importance of the parameters may also vary from one watershed to another [24]. Hence, it is important to perform a sensitivity analysis to elucidate which parameters are more influential and in what range their influence is significant.

Arid regions present the hydrologic modeler with several challenges. They are often ungauged or poorly gauged with scarce precipitation as well as other model input data. They also lack ground observations of flood depth and flow due to extreme rainfall events. This has resulted in limited investigations on using IMERG SPPs in flash flood modelling in arid regions. The UAE is no exception, as only a few publications investigated the recent

trends of precipitation extremes [25,26]. There is also a lack of a detailed investigation on the relative influence of model input parameters on the accuracy of simulated flash flood events in arid regions, particularly in the UAE. Hence, the present study aims to (1) evaluate the recent trends of precipitation extremes related to floods in the UAE, (2) evaluate the accuracy of the different IMERG products compared to using ground observations in the hydrological modelling of flash flood events in UAE, and (3) highlight the parameters that influence the output of hydrological models developed in arid regions through a sensitivity analysis.

2. Study Area and Data

2.1. Study Area

Figure 1 shows the map of the United Arab Emirates (UAE) and the locations of the three watersheds (wadis). The UAE lies in the Arabian Peninsula between 22°40′ and 26°00′ North and 51°00′ to 56°00′ East. The UAE has no perennial rivers but many wadis that are permanently or intermittently dry. Three wadis, namely Wadi Taween, Wadi Maidaq, and Wadi Ham, were selected for the present study. All these three wadis are located in the northeastern part of the UAE. These wadis were chosen because they had received relatively higher rainfall than other regions of the UAE [27]. Moreover, the northern part of the UAE experienced frequent flash flood events [27,28]. Hence, many retention and detention dams have been constructed around these wadis for groundwater recharge and surface water harvesting [28]. Wadi Ham encountered the highest storm in March 1900, which led to maximum storage of surface water up to 4.87 M m^3 in its dam [27]. Similarly, Wadi Taween encountered the highest storm in March 1998, which led to maximum storage of 3.50 M m^3 in Wadi Taween dam [27]. Also, the three wadis exist in a mountainous region with rocky soil, and during a storm event, only a small portion of the rain infiltrates into the mountain beds. Thus, even though these wadis remain dry for most of the year, they can convey a large volume of flood water during extreme rainfall events [29]. Here, extreme rainfall events refer to unusually high intensity, duration, or magnitude compared to the typical or average rainfall patterns observed in a region. The slope and characteristics add to the probability of flash floods in the downstream plains of these wadis. More importantly, urban areas exist in the flood plains of these wadis and have witnessed severe damage to the built environment during flood events that often occur during the winter months of November to March [27].

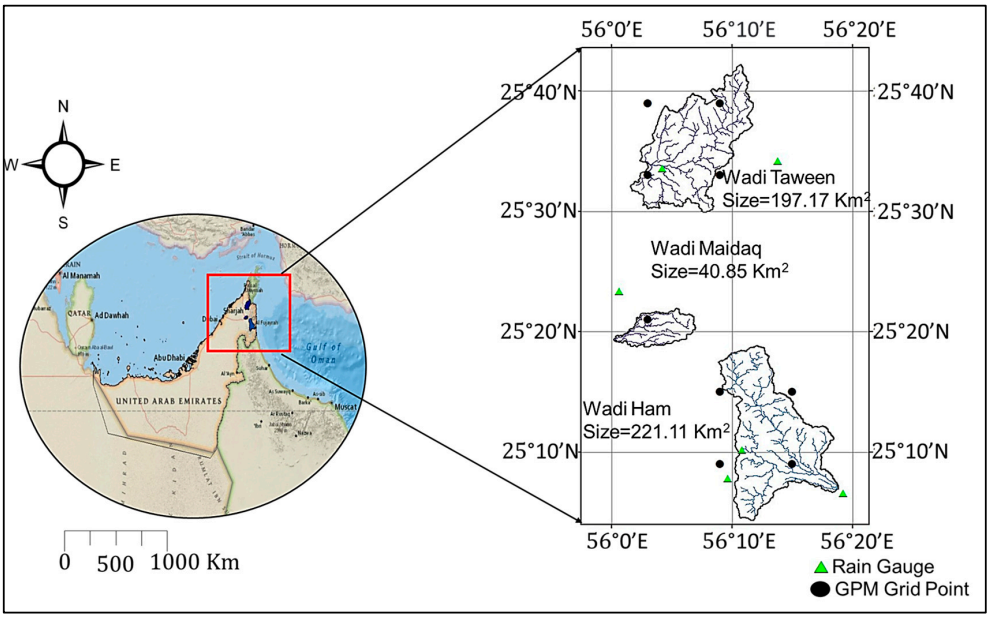

Figure 1. Geographical locations and areas of the selected wadis with rain gauge data obtained from the National Centre of Meteorology, UAE, and the corresponding GPM IMERG grid points.

2.2. Rain Gauge Data and GPM IMERG Satellite Precipitation Products

Rainfall data from six rain gauge stations located around the three selected watersheds were obtained from the National Centre of Meteorology (Table 1). Accordingly, GPM IMERG products, V06, around the three watersheds were downloaded. The GPM IMERG half-hourly products were downloaded from NASA Precipitation Processing System (PPS) (https://pmm.nasa.gov/data-access/downloads/gpm, accessed on 17 November 2022). Three IMERG products, namely IMERG Early, IMERG Late, and IMERG Final, were downloaded for hydrological modelling based on the date of the extreme event. The half-hourly IMERG products were aggregated into a daily product. This aggregation was performed to match the temporal resolution of IMERG data with that of gauge data, allowing for consistent comparison and analysis. For IMERG Final, a daily time series from 2001 to 2020 was also downloaded for trend analysis. IMERG Final was selected because it had the best performance over the study area in a previously published point-to-point evaluation [14]. An algorithm written in R was used to extract and process the IMERG data. The script converted the IMERG data to ASCII format and adjusted it by 4 h. The adjustment of IMERG data by 4 h refers to shifting the original time stamps of the data by 4 h. This adjustment is made to align the time stamps with the local time zone in the UAE region. By making this adjustment, the data can be properly compared with rain gauge observations. A coordinate matching algorithm was then employed to match the IMERG grid point with the nearest rain gauge station. Details of the analysis can be found in Mohammed et al. [14]. The locations of the six rain gauges and IMERG grid intersections are shown in Figure 1. A preliminary data analysis was conducted to select the dates of the extreme event. A combination of statistical methods, such as identifying the maximum value of the rainfall data series, and visual analysis, specifically using histograms, was used to identify the dates of the extreme event. The period between 9 and 12, January 2020, was identified as an extreme event, as it caused flooding, blocked roads, and damaged properties in many parts of the UAE. Therefore, 9 to 12 January 2020 was chosen as an extreme event date for hydrological modelling.

Table 1. GPS location and name of the rain gauge stations (obtained from the National Centre of Meteorology, UAE).

Latitude	Longitude	Station Name	Wadi	Frequency of Data	Dates	Distance to Nearest GPM (Km)
25.39	56.01	Manama	Wadi Maidaq	Daily	2017–2020	5.8
25.17	56.18	Al FarFar	Wadi Ham	Daily	2017–2020	3.6
25.13	56.16	Al Heben	Wadi Ham	Daily	2017–2020	2.2
25.11	56.32	Fujairah Int'l Airport	Wadi Ham	Daily	2017–2020	8.1
25.56	56.07	Al Tawiyen	Wadi Taween	Daily	2017–2020	2.3
25.57	56.23	Dibba	Wadi Taween	Daily	2017–2020	8.0

3. Methodology

This study is divided into three parts. The first part evaluates recent trends in precipitation extremes related to floods in the three wadis. It is important to identify any increase in the frequency and intensity of extreme rainfall events, which are often attributed to climate change. In the second part, the accuracy of the different IMERG products is compared to ground observations in the hydrological modelling of a recent flash flood event. This analysis is critical for un-gauged areas to determine the reliability of IMERG products in flash flood modelling and prediction. The third and final part of the analysis highlights the parameters that influence the hydrological model output through a sensitivity analysis. This is important to elucidate the parameters that are most influential in arid mountainous regions, similar to the selected wadis. The overall flowchart of the methodology is shown in Figure 2.

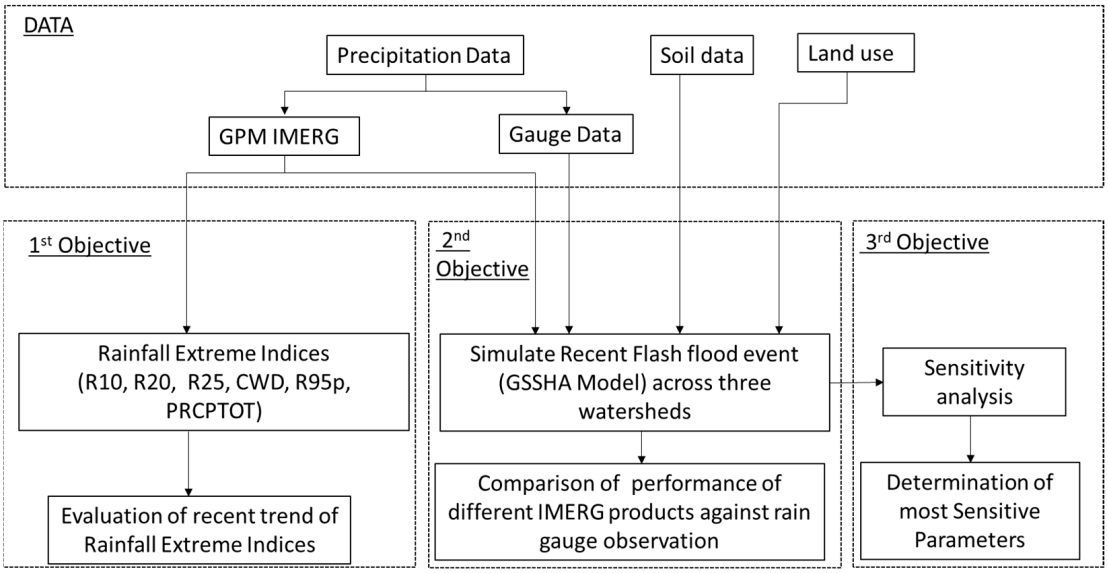

Figure 2. Overall Methodology.

3.1. Trends of Extreme Rainfall Indices

Rainfall indices related to flood were calculated from the processed GPM Final run product daily time series (2001–2020). This product was selected as it performed best over the study area in a previously published point-to-point evaluation [14]. Gauge data were not used because of the lack of long-term daily data. Also, as IMERG is not a climate data record, the present study incorporated CHIRPS (Climate Hazards Group InfraRed Precipitation with Station data) into the analysis [15]. CHIRPS is a satellite-based rainfall dataset developed by the Climate Hazards Group at the University of California, Santa Barbara [30]. It combines infrared satellite data with ground-based station observations to provide high-quality precipitation estimates on a global scale. In terms of resolution, CHIRPS data are available at a spatial resolution of 0.05 degrees (approximately 5 km) and on a daily timescale. CHIRPS is widely used for climate studies and provides gridded precipitation estimates by combining satellite imagery and ground station observations [31,32]. To compare the trends in precipitation extreme indices between the IMERG Final and CHIRPS datasets, the CHIRPS data were extracted at the coordinates of the corresponding IMERG Final data. Both datasets were analyzed using the same daily time series from 2001 to 2020 to ensure temporal consistency. By aligning the spatial and temporal dimensions, this approach enables a direct comparison of precipitation extremes and facilitates an assessment of trends across the datasets.

Six recognized extreme rainfall indices commonly reported in the literature [33,34] were selected and evaluated based on guidelines published on the world meteorological website (www.wmo.int, accessed on 17 February 2022). Table 2 shows the description and units of the selected indices. In the study, the authors used RClimDex, an R-language-based software package version 1.8-2 by the Expert Team for Climate Change Detection Monitoring and Indices (ETCCDMI), to determine the extreme precipitation indices [35]. RClimDex not only calculates the extreme precipitation indices but also provides a precipitation data homogeneity test. This test helps ensure the consistency and reliability of the precipitation data used in the analysis [35]. By conducting the homogeneity test, the authors can assess whether the precipitation data exhibits any significant changes or inconsistencies over time, which could potentially affect the results of the extreme precipitation indices.

Table 2. Selected indices for analysing trends of rainfall extremes from the RClimDex software package version 1.8-2.

Index	Unit	Description
R10	Days	Annual count of days when precipitation $\geq$ 10 mm
R20	Days	Annual count of days when precipitation $\geq$ 20 mm
R25	Days	Annual count of days when precipitation $\geq$ 25 mm
CWD	Days	Maximum number of consecutive days with RR $\geq$ 1 mm
R95p	mm	Annual total PRCP when RR > 95th percentile
PRCPTOT	mm	Annual total PRCP in wet days (RR $\geq$ 1 mm)

The Mann–Kendall method [36] is a widely used statistical test for detecting trends in hydrological variables, such as rainfall and streamflow. However, one limitation of the standard Mann–Kendall test is that it assumes that the data points in the time series are independent, which may not be the case in many hydrological applications due to autocorrelation in the data [33]. To address this issue, a modified version of the Mann–Kendall test has been developed that takes into account the autocorrelation in the data [37]. This modified test is also known as the Modified Mann–Kendall (MMK) test [37]. The MMK test includes a revised variance value, accounting for the data set's autocorrelation. The modified variance is as follows:

$$Var \times (S) = Var\ (S) \times \left(\frac{n}{n_e^*}\right) = \left(\frac{n\ (n-1)(2n+5)}{18}\right)\left(\frac{n}{n_e^*}\right), \quad (1)$$

where n denotes the actual sample size, n_e^* represents the effective sample size and $\left(\frac{n}{n_e^*}\right)$ represents the correlation due to autocorrelation and is calculated as:

$$\left(\frac{n}{n_e^*}\right) = 1 + \left(\frac{2}{n\ (n-1)(n-2)}\right)\sum_{i=1}^{n-1}(n-f)(n-i-1)(n-i-2)\rho_e(i) \quad (2)$$

$\rho_e(i)$ represents the autocorrelation functions of the rank of the observation. Details about the MMK can be found in Hamed et al. [37].

The nonparametric MMK test was used in this study to evaluate the trends of the extreme rainfall indices. The test results can indicate whether the trend is significantly decreasing, increasing, or has no significant trend. A significance level of 0.05 was considered for the analysis. Thus, a significant trend is detected by the MMK test as either increasing or decreasing with a p-value less than the chosen significance level ($p < 0.05$). In other words, a simple positive or negative trend refers to a general increasing trend or decreasing trend in the data without specifically referring to statistical significance. It indicates a visually observable pattern of increasing or decreasing values over time but without rigorous statistical analysis to determine if the trend is statistically significant. On the other hand, a significant positive or negative trend ($p < 0.05$) denotes statistical significance.

3.2. Hydrological Modelling

According to the National Center of Meteorology (NCM), UAE recorded the highest rainfall between 9 and 12 January 2020, which broke the record for the highest amount of rain received in the UAE since 1996. The event was reported to cause flooding, blocked roads, and damaged properties in many parts of the UAE, including the northern regions. In view of this, the present study utilizes version 11.1 of the Watershed Modelling System to implement the Gridded Surface Subsurface Hydrologic Analysis (GSSHA) model and simulate the storm event that occurred from 9 to 12 January 2020 in the three wadis. GSSHA is a physical-based distributed hydrological model that simulates the response of a watershed to a specified hydrometeorological input. The GSSHA model partitions the entire watershed into uniform finite-difference grid cells and subsequently evaluates the

hydrological processes occurring during and after a rainfall event at each grid cell. These processes are then aggregated to determine the overall response of the entire watershed.

GSSHA can rely on one of two methods to distribute the rainfall uniformly over the basin: Thiessen Polygon and Inverse Distance Squared Weighting (IDW). Each method has its own set of advantages and disadvantages. One of the drawbacks of the Thiessen Polygon method is its sensitivity to gauge density and the distribution of rain gauges [38]. Since there are a limited number of IMERG grid points and rain gauges available for the study area, the IDW method was considered more appropriate. IDW estimates rainfall at unsampled points by considering a linear combination of rainfall values at known points, weighted by an inverse function of the distance from the point of interest. This method allows for the interpolation of rainfall data based on the available observations without relying heavily on the density or distribution of rain gauges. More details about IDW can be found in Chen et al. [39]. Similarly, there are four available methods to simulate infiltration in GSSHA. These methods are: The Green and Ampt (GA), the Green and Ampt with Redistribution (GAR), the fully implemented Richards's equation, and the multi-layered GA. In this study, the GAR method was used to simulate infiltration. GAR is based on the following equation:

$$f(t) = K\left(\frac{S_f(\theta_s - \theta_i)}{F(t)} + 1\right) \tag{3}$$

where:

$f(t)$ = Potential infiltration rate (cm/hr).
K = Effective hydraulic conductivity (cm/hr).
$F(t)$ = Cumulative infiltration (cm).
S_f = Wetting front suction head (cm).
θ_i = Initial soil moisture content.
θ_s = Soil moisture content at natural condition.

After subtracting all abstraction, the amount of water ponded over each grid cell was then computed and routed into two orthogonal directions using a diffusive wave approximating St. Venant's equation. The watershed boundary served as a no-flow boundary; thus, the flow is not routed outside the watershed boundary. Again, there are different numerical schemes in GSSHA to solve the diffusive wave equation. The present study uses the Alternative Direction Explicit (ADE) to route the flow. The overflow that enters the stream is routed up to the outlet of the watershed.

As per the ADE method, $\Delta x = \Delta y$. First the interflow was calculated in the x direction as follows:

$$P_{ij}^N = \frac{1}{n}\left(d_{ij}^N\right)^{5/3}\left(s_{fx}^N\right)^{1/2} \tag{4}$$

Based on the flow, the depth at the $n + 1$ time interval in the x direction was calculated as:

$$d_{ij}^{N+1/2} = d_{ij}^N + \frac{\Delta t}{\Delta x}\left(p_{i-1,j}^N - p_{ij}^N\right) \tag{5}$$

Then, the interflow in the y-direction was calculated using the updated depth as follows:

$$q_{ij}^{N+1/2} = \frac{1}{n}\left(d_{ij}^{N+1/2}\right)^{5/3}\left(s_{fy}^{N+1/2}\right)^{1/2} \tag{6}$$

Then, depth in each y column was calculated as:

$$d_{ij}^{N+1} = d_{ij}^{N+1/2} + \frac{\Delta t}{\Delta x}\left(q_{i,j-1}^{N+1/2} - q_{ij}^{N+1/2}\right) \tag{7}$$

The volume of flow at each node was calculated as:

$$V_i^{N+1} = V_i^N + \Delta t\left(q_{lat}^{N+1}\Delta x + q_{rec}^{N+1}\Delta x - Q_{i-1/2}^N - Q_{i+1/2}^N\right) \tag{8}$$

where:

p_{ij} = Overflow in x directions from cell ij.
q_{ij} = Overflow in y directions from cell ij.
d_{ij} = Depth of water in cell ij at Nth time.
n = Manning's roughness coefficient.
S_{fx} = Water surface slope in the x direction.
S_{fy} = Water surface slope in the y direction.
q_{lat} = Lateral flow.
q_{rec} = Flow exchange between groundwater and the surface.

3.2.1. Model Inputs

GSSHA uses the Digital Elevation Model (DEM) to delineate the watershed and stream networks. For this study, the DEM at 30 m resolution was obtained from Shutter Radar Topography Mission (SRTM) and projected to Universal Transverse Mercator zone 40N. The LULC data at a 10 m resolution were obtained from the ESRI data portal [40] for 2020. This global LULC data, which were generated from ESA Sentinel 2 imagery, contained misclassifications for some land use categories in the study area. To address this issue, ground observations and Google Earth images were used to reclassify the LULC data. For example, areas previously classified as flooded vegetation were reclassified as bare land, etc. The LULC of these wadis showed that the majority of the watershed is of barren land composed of mountain rocks and sand (Figure 3). The soil type data required for the GSSHA model were obtained from Environment Agency Abu Dhabi (EAD) in the form of a shapefile, which had a Scale Factor of 0.99. The data showed that most of the soil type is mountainous rocks (Figure 4). Tables 3 and 4 show the infiltration parameters and the overland flow of the watershed used to run the GSSHA model. These values were extracted from the published literature and from the GSSHA manual [21,41].

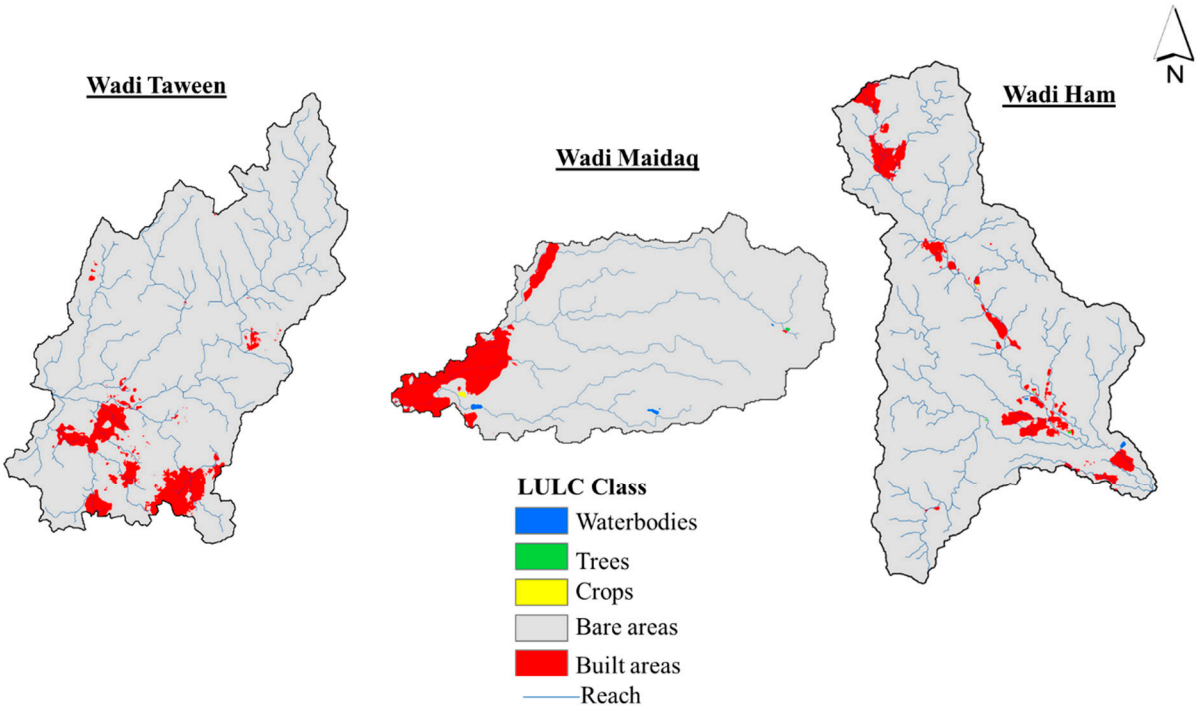

Figure 3. Land use and land cover type for the three wadis derived from ESA Sentinel 2 imagery and reclassified based on ground observation and google earth imagery.

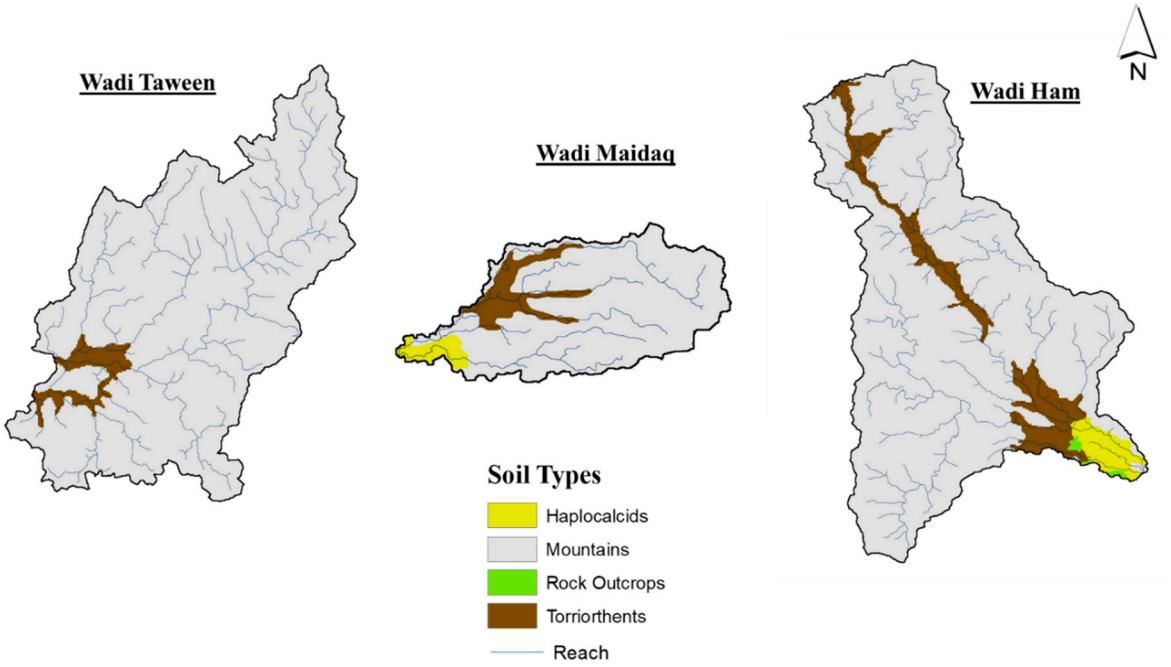

Figure 4. Soil type of the three wadis obtained from Environment Agency Abu Dhabi (EAD).

Table 3. Infiltration parameters of the watersheds.

Soil Type	Soil Texture	Hydraulic Conductivity (cm/h)	Effective Porosity	Capillary Head (cm)	Initial Moisture Content
Rock outcrops	Rock	0.0002 [a]	0.2 [a]	10 [a]	0.011 [a]
Torriorthents	Sandy loam	1.09 [b]	0.453 [b]	11.01 [b]	0.095 [a]
Mountains	Rock	0.0002 [a]	0.2 [a]	10 [a]	0.011 [a]
Haplocalcids	Sandy loam	1.09 [b]	0.412 [b]	11.01 [b]	0.095 [a]

Source of data: [a] = Al-Areeq et al. [21] and [b] = GSSHA manual [41].

Table 4. Overland flow parameters of the watersheds.

Land Use Type	Manning Roughness Coefficient
Waterbodies	0.05
Trees	0.3
Crops	0.22
Built area	0.1
Bare area	0.2

Source of data is from Al-Areeq et al. [21] and the GSSHA manual [41].

3.2.2. Performance of IMERG Data in Simulating Storm Events

The ability of different IMERG products to simulate the 9 to 12 January 2020 storm event for the three watersheds was assessed using standard statistical measures. These statistical measures are expressed as follows:

$$\text{Root Mean Square Error (RMSE)} = \sqrt{\frac{\sum_{i=1}^{n}(G_i - I_i)^2}{n}}$$

$$\text{Mean absolute Error (MAE)} = \frac{\sum_{I=1}^{n} abs\,(G_i - I_i)}{n}$$

$$\text{Percentage of Peak error, } E_{peak}\,(\%) = \frac{P_G - P_I}{P_G} \times 100$$

$$\text{Percentage of Volume error, } E_{\text{volume}}\ (\%) = \frac{V_G - V_I}{V_G} \times 100$$

where:

G_i = Streamflow (m^3/s) using gauge rainfall data.
I_i = Streamflow (m^3/s) using rainfall data obtained from IMERG.
$\overline{O}$ = average observation value.
P_G = Peak flow (m^3/s) using gauge rainfall data.
P_I = Peak flow (m^3/s) using rainfall data obtained from IMERG.
V_G = Peak volume (m^3) using gauge rainfall data.
V_I = Peak volume (m^3) using rainfall data obtained from IMERG.

The RMSE measures the average magnitude of the differences between predicted and observed values, giving higher weight to larger errors due to the squaring operation, making it more sensitive to outliers [42,43]. On the other hand, the MAE measures the average magnitude of the differences between predicted and observed values, being less sensitive to outliers since it does not square the errors before averaging them [42,43]. The Percentage of Volume Error quantifies the difference between the total volume of predicted and observed values as a percentage of the observed total volume. It indicates how well the model captures the overall volume or total amount of the observed data, with a lower percentage indicating a closer match between the predicted and observed total volumes. Similarly, the Percentage of Peak Error measures the difference between the peak values of predicted and observed values as a percentage of the observed peak value. It provides an indication of how well the model captures the peak magnitude of the observed data, with a lower percentage indicating a closer match between the predicted and observed peak values.

3.3. Sensitivity Analysis of the GSSHA Model to Input Parameters

A sensitivity analysis of the model output under varying input parameters was carried out using a one-factor-at-a-time method [44]. Using this method, each of the GSSHA input parameters was increased and decreased three times by a factor of 20% from its base value while keeping all other values constant [45]. Then, the corresponding change in the volume at the watershed outlet was computed. Based on the volume changes, the relative sensitivity of the output to model input was evaluated, and consequently, the input parameters were ranked. The relative sensitivity coefficient was calculated based on the formula suggested by Saha et al. [45], as follows:

$$\text{Relative Sensitivity Coefficient (RSC)} = \frac{(M_a - M_n)/M_n}{(P_a - P_n)/P_n}$$

where:

P_a and M_a = parameter changing value and model output (volume) after running the model using parameter changing value.
P_n and M_n = parameter base value and model output (volume) using parameter base value.

4. Results

4.1. Comparison of Trends in Extreme Precipitation Indices Using IMERG Final and CHIRPS

Table A1 in Appendix A shows the comparison of trends using IMERG Final and CHIRPS data sets. It can be observed that the trends in precipitation extreme indices from both IMERG Final and CHIRPS datasets generally exhibit consistency across most locations. The majority of indices analyzed, such as R10, R20, R25, CWD, R95, and PRCPTOT, show similar trends in both datasets, indicating agreement and reliability in their observations. The similarities between IMERG and CHIRPS in capturing precipitation extremes can be attributed, in part, to their utilization of station data, albeit from different sources. The

use of station data may contribute to the overall alignment of the trends observed in the two datasets. However, there are a few instances where IMERG and CHIRPS show slight discrepancies in the nature of the trend. In some cases, IMERG may indicate a significant positive trend, while CHIRPS shows a simple positive trend. These differences could be attributed to the specific characteristics and algorithms used in each dataset, as well as the spatial and temporal resolutions. IMERG relies on passive microwave satellites, whereas CHIRPS primarily utilizes infrared sensors. These differences in data sources and sensing techniques can influence the observed discrepancies in trends between the two datasets.

Overall, the comparative analysis demonstrates the usefulness of incorporating CHIRPS data to validate the trends observed in IMERG. The consistent trends observed between the two datasets provide confidence in the reliability of the results and enhance our understanding of precipitation patterns and trends over the study area. It is important to note that further investigation and consideration of other factors, such as changes in the observing constellation and potential artifacts, should be taken into account when interpreting the trends obtained from IMERG and CHIRPS.

4.2. Recent Trends in Extreme Precipitation Indices Using IMERG Data

The result of the trend analysis showed an increasing trend for the majority of the indices (Figures 5–7). The number of days with more than 10 mm of rainfall significantly increased in Wadi Ham. Although not statistically significant, an increasing trend was also observed in Wadi Taween and Wadi Maidaq. Similarly, the annual total precipitation was statistically significant in Wadi Ham. In contrast, consecutive wet days were statistically significant in a few stations of Wadi Taween and Wadi Maidaq. Although not significant, the number of days with more than 25 mm of rainfall was also found to follow an increasing trend except in one of the grid points in Wadi Ham, where no trend was noted (Figure 5).

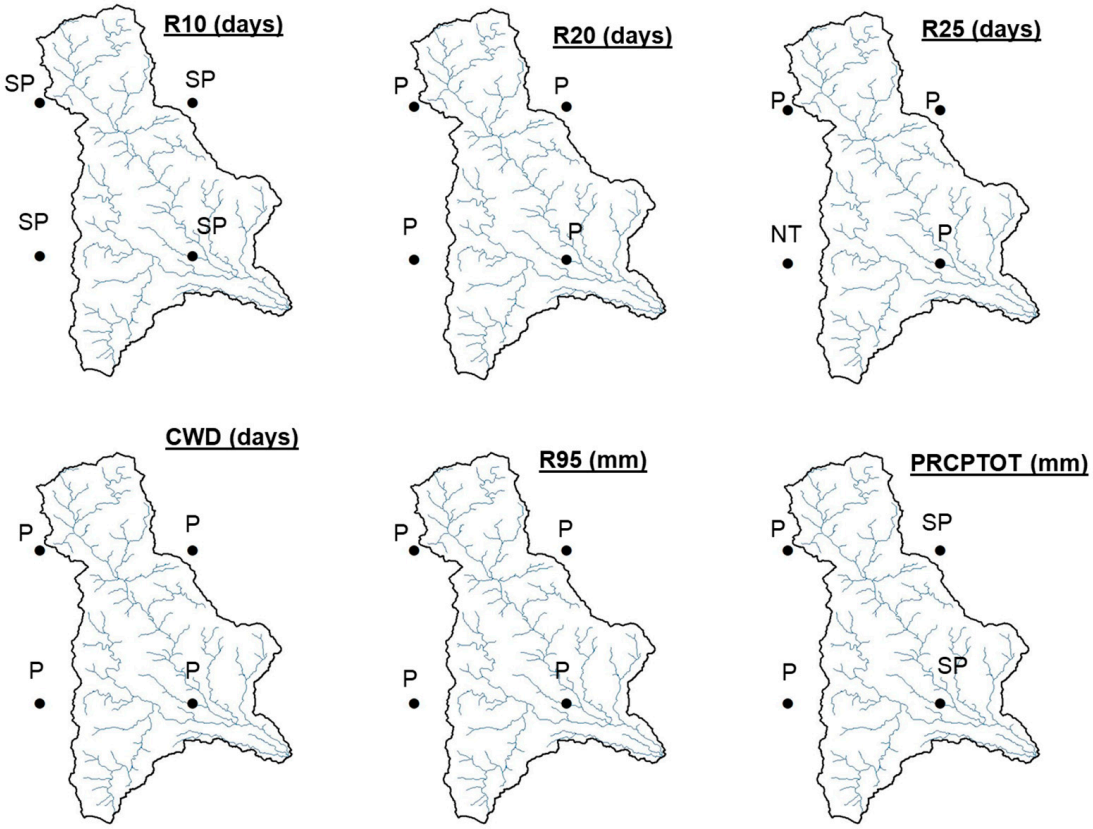

Figure 5. Trends for various extreme precipitation indices at Wadi Ham on the IMERG grid point (The abbreviations are NT = no trend, P = positive trend, SP = significant positive trend, N = negative trend, and SN = significant negative trend).

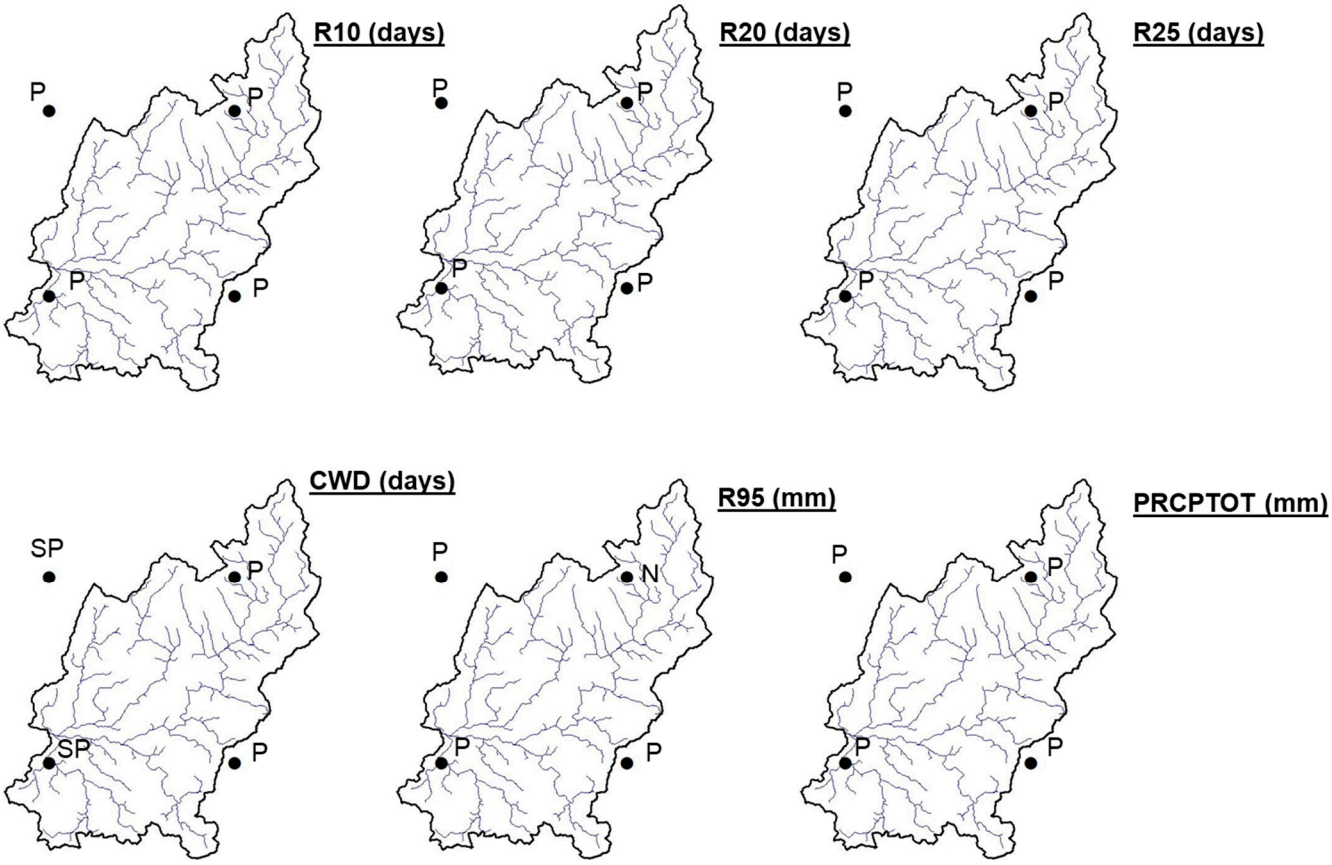

Figure 6. Trends for various extreme precipitation indices at Wadi Taween on the IMERG grid points (The abbreviations are NT = no trend, P = positive trend, SP = significant positive trend, N = negative trend, and SN = significant negative trend).

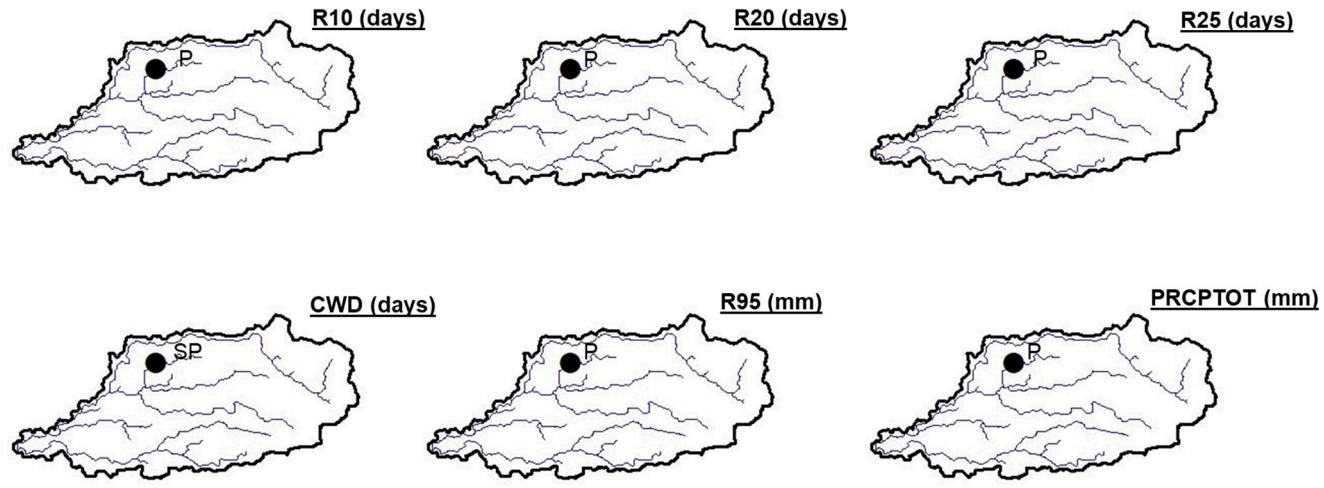

Figure 7. Trends for various extreme precipitation indices at Wadi Maidaq on the IMERG grid point (The abbreviations are NT = no trend, P = positive trend, SP = significant positive trend, N = negative trend, and SN = significant negative trend).

4.3. Performance of IMERG Products in Hydrological Modelling of Extreme Event

The predicted outlet hydrographs when the GSSHA model was forced by the gauge rainfall and the three IMERG products are shown in Figures 8–10. The timing of streamflow captured by the GSSHA model depends on several factors, including the time step used in the simulation, the accuracy of input data, and the complexity of the hydrological processes

being simulated. In this study, both the gauges and IMERG data are at a daily time scale, so the observed streamflow variations are captured at a daily time scale. However, the GSSHA model was operated at a finer time scale, with a time step of 60 min. This allows for more detailed variations in streamflow to be captured, including rapid changes that may occur within a day. By using this finer time step, the GSSHA model aims to represent the timing of streamflow events more accurately.

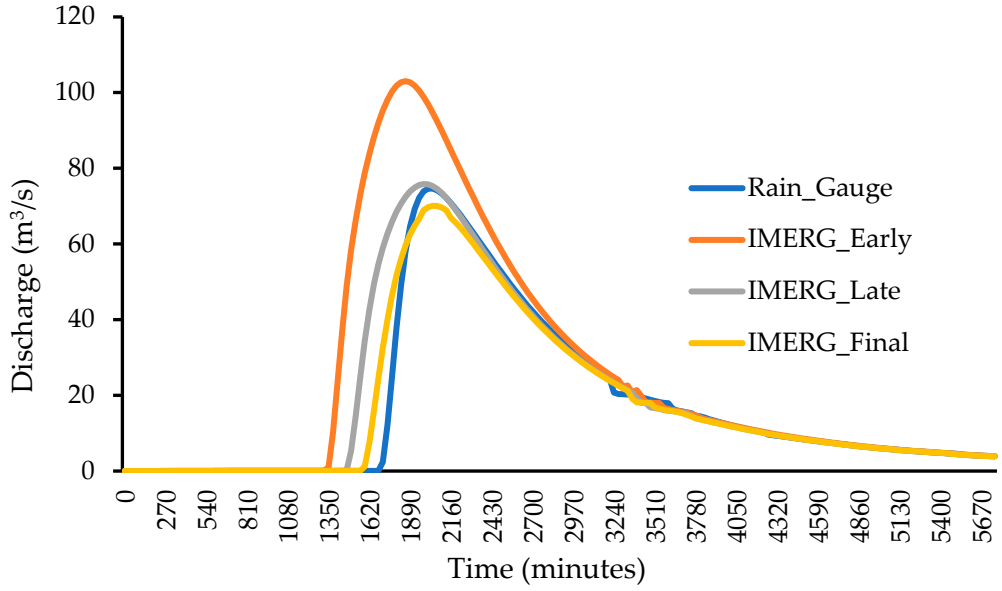

Figure 8. Simulated hydrograph for the 9–12 January event at the outlet of Wadi Ham driven by the three IMERG products and gauge rainfall data.

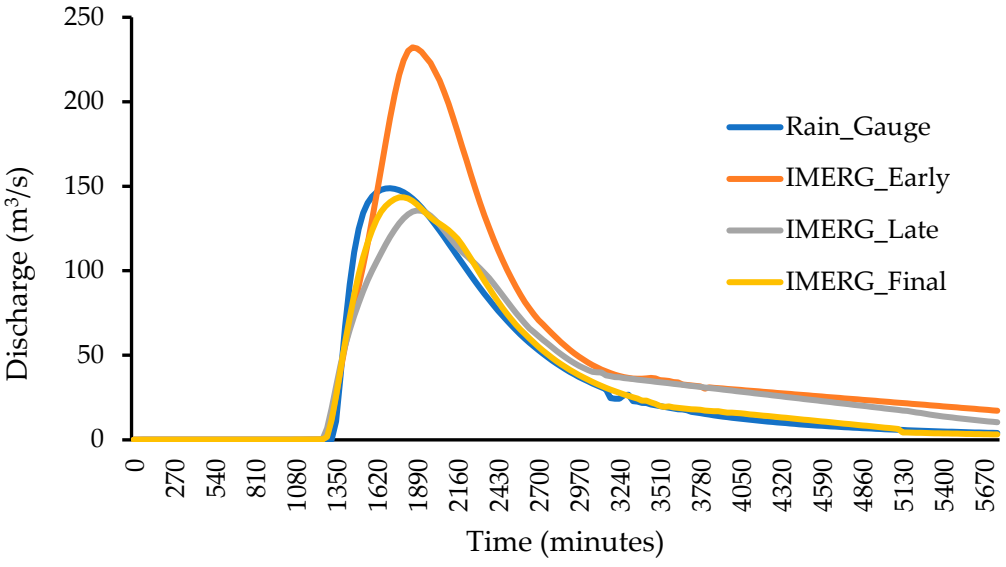

Figure 9. Simulated hydrograph for the 9–12 January event at the outlet of Wadi Taween driven by the three IMERG products and gauge rainfall data.

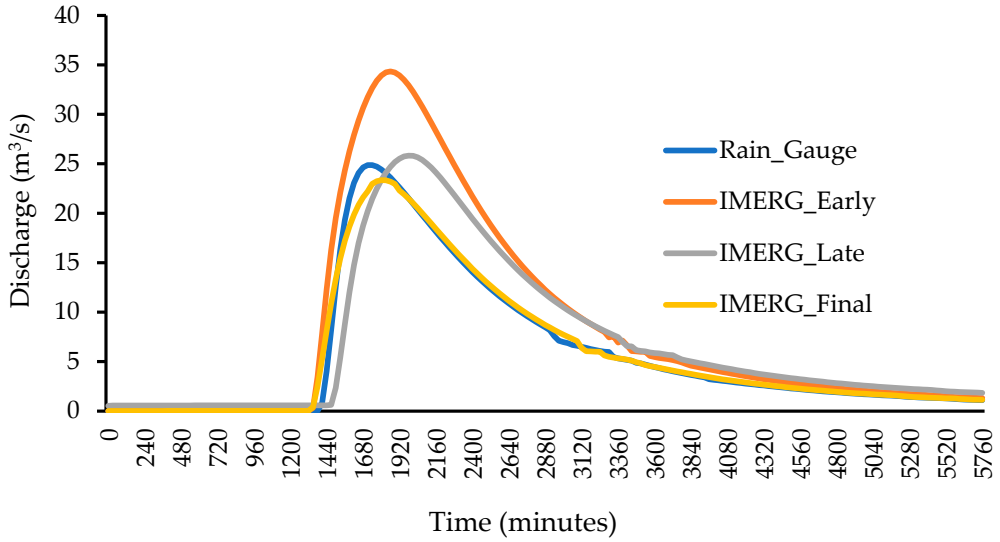

Figure 10. Simulated hydrograph for the 9–12 January event at the outlet of Wadi Maidaq driven by the three IMERG products and gauge rainfall data.

There is no observed streamflow recorded; however, as the aim was to test the accuracy of IMERG products, the author assumed that the streamflow generated by the gauge rainfall data as the true streamflow value. Therefore, the output hydrograph obtained when the model was run with three IMERG products was finally compared with the model output when run with rainfall gauge data. As seen in Figure 8, the IMERG early run significantly overestimated the outlet discharge of the Wadi Ham watershed. IMERG late performed better than IMERG early. Whereas the hydrograph from the IMERG final product closely matches the hydrograph generated using gauge data. Similar trends were observed for Wadi Taween and Wadi Maidaq (Figures 9 and 10). Table 5 summarizes the quantitative accuracy of the three IMERG products against the gauge data in driving the GSSHA model for all three wadis. Table 5 shows the superiority of final IMERG products with respect to other IMERG products in terms of MAE, RMSE, and peak and volume errors for all three wadis. All three IMERG products were found to underestimate the flood volume, where the percentage of volume error was negative for all three wadis (Table 5). Regarding Peak flow, IMERG early tends to overestimate the peak value, whereas the IMERG final tends to underestimate the peak value for all three wadis. Overall, the highest errors were found in the case of wadi Ham, followed by Wadi Taween and Wadi Maidaq. Interestingly, the error was positively correlated to the size of the wadis. Wadi Ham has the highest catchment area (221.11 Km^2), followed by Wadi Taween (197.17 Km^2), and Wadi Maidaq (40.85 Km^2).

Table 5. Hydrological performance of the three IMERG products for the 9–12 January event.

Wadi	Rainfall Type	Statistical Measures			
		E_{peak} (%)	E_{volume} (%)	MAE	RMSE
Wadi Ham	Gauge vs. IMERG Early	−38.02	−44.92	7.74	20.95
	Gauge vs. IMERG Late	−1.6	−12.76	2.73	9.8
	Gauge vs. IMERG Final	6.11	−0.90	1.5	4.36
Wadi Taween	Gauge vs. IMERG Early	−56.04	−54.07	19.59	29.43
	Gauge vs. IMERG Late	8.8	−16.03	10.26	13.62
	Gauge vs. IMERG Final	3.59	−1.39	2.97	5.59
Wadi Maidaq	Gauge vs. IMERG Early	−3.83	−43.20	2.48	4.193
	Gauge vs. IMERG Late	−38.02	−21.01	2.09	3.01
	Gauge vs. IMERG Final	6.11	−0.56	0.50	0.79

4.4. Sensitivity Analysis of the Model to Input Parameters

Table 6 shows that five parameters out of all the parameters used to run the GSSHA model significantly influenced the model's output. The other parameters had very little influence, hence, they are not displayed in the table. The parameters were run for different soil types and land use types (as shown in Tables 3 and 4). Hence, KS (mountain) refers to the hydraulic conductivity of the mountain's soils, and Manning's *n* (built areas) refers to Manning's coefficient for built-up areas.

Table 6. Parameter sensitivity and their ranking based on influence on flood volume at the watershed outlet.

Wadi Ham			Wadi Taween			Wadi Maidaq		
Parameter	**Relative Sensitivity**	**Rank**	**Parameter**	**Relative Sensitivity**	**Rank**	**Parameter**	**Relative Sensitivity**	**Rank**
Porosity (mountain)	0.017	1	KS (mountain)	0.021	1	Porosity (mountain)	0.0019	1
KS(mountain)	0.013	2	Porosity (mountain)	0.019	2	KS (mountain)	0.0016	2
Capillary Head (mountain)	0.012	3	Capillary Head (mountain)	0.016	3	Capillary Head (mountain)	0.0013	3
Manning's *n* (Built area)	0.009	4	Manning's *n* (Bare area)	0.008	4	Manning's *n* (Built area)	0.009	4
Manning's *n* (Bare area)	0.007	5	Manning's *n* (Built area)	0.006	5	Manning's *n* (Bare area)	0.005	5

KS: Hydraulic conductivity.

5. Discussion

The result of the trend analysis gives a clear indication of increasing trends of extreme rainfall events in the three watersheds of the UAE. Thus, it was logical to find that rainfall was the most important factor affecting the UAE's wadis [24]. Hence, the increasing trend of these extreme rainfall indices likely suggested that these wadis have been subjected to more frequent flash floods in recent years, as these wadis can be flooded with even a small amount of precipitation [24]. The finding of this study is consistent with other studies that have shown an increasing trend towards more extreme rainfall in the UAE and Gulf regions. For instance, Choudhary et al. [26] found a statistically significant increasing trend in extreme temperature and rainfall parameters in all locations of the northeastern part of UAE except in the Al Ain region. A previous study also suggested a likely increase in extreme rainfall and temperature trends for the UAE [24]. The findings underscore the need for more detailed hydrological modelling to simulate and predict the impact of flash flood events and develop strategies to mitigate the identified risks.

The GSSHA model was run to simulate the highest rainfall between 9 and 12 January 2020 that occurred in UAE. The study found that the IMERG final product was the closest match to the gauge data. The study also found that the size of the catchment areas influenced the propagation of errors from IMERG products to the model output. The highest errors were found in the case of the largest catchment area, Wadi Ham, followed by Wadi Taween and Wadi Maidaq. This is in agreement with the findings of several authors who reported that the improvement of the hydrological model is a direct function of its catchment areas [2,36,37]. This signifies that the size of the wadis may influence the propagation of the errors from IMERG products to the model output [2]. However, it is possible that the apparent higher errors in the case of the largest catchment area could also be attributed to the limited number of available gauges and their representativeness of larger wadis. To provide a more comprehensive and accurate understanding of the relationship between catchment size and error propagation, further analysis and investigation are required. Future studies could consider additional factors such as gauge distribution, representativeness, and spatial heterogeneity within the larger catchment areas. The main limitation of this study is that the developed model was not calibrated with ground measurements of discharge. However, this is the case for many flash floods,

where the discharge data are often unavailable. Nevertheless, the outcome of this analysis highlighted the magnitude of error (in this case, the difference between the raw satellite data and gauge data) to be expected when using the different raw IMERG products. The finding thus highlighted the potential of IMERG's final product and the need to carry out bias correction and other analyses to improve its performance before its application for flash flood prediction/modelling in similar wadis.

The sensitivity of the GSSHA model output to various input parameters was analyzed. Out of the five most influencing parameters, three parameters, namely porosity, hydraulic conductivity (KS), and capillary head, control the infiltration, while Manning's coefficient controls the stream flow routing. Porosity, which refers to the percentage of void space, had the highest relative sensitivity in Wadi Ham and Wadi Maidaq, as the majority of the watershed is made up of mountain soil. While in the case of Wadi Taween, hydraulic conductivity, which refers to the property of the soil to transmit water through pore space, was the most influential parameter. Thus, it can be concluded that the infiltration parameters are the most influential parameters in the study area. These findings are consistent with previous studies that have highlighted the importance of infiltration parameters in hydrological modelling [46,47]. However, more future studies are needed to confirm the importance of these parameters in arid watersheds. Future studies should also assess the sensitivity of the GSSHA model to the resolution of digital topographic models, grid cell size, and stream density, as these factors are critical to the model's performance [48]. One limitation to this finding, though, is that the values of the parameters used in this study were obtained from literature and the GSSHA manual. Thus, future studies in similar arid regions should obtain accurate values for these input parameters through field measurements to increase confidence in the model's performance.

6. Conclusions

The study evaluates the trend in extreme rainfall events in three watersheds in the UAE. Findings show that the number of days with more than 10 mm of rainfall, annual total precipitation, and consecutive wet days have increased, indicating an increased risk of flooding in these areas. The study also evaluated the performance of three IMERG products in predicting flood events and found that the IMERG final product performed well when compared to gauge rainfall data. However, more ground data are needed to confirm this in future studies. Results of the sensitivity analysis indicated that infiltration parameters significantly influenced model outputs in the study area. Similar studies are needed to confirm the parameters that influence the predictive accuracy of watershed models in arid regions. Investment in obtaining high-accuracy ground data for these influential parameters can help to improve the accuracy of flash flood prediction models and mitigate the risk of flooding.

Author Contributions: Conceptualization, M.A.H., G.H. and M.M.M.; Data curation, M.A.H. and G.H.; Formal analysis, H.S.Y., H.A.M. and M.M.; Funding acquisition, M.A.H. and M.M.M.; Investigation, G.H., H.S.Y., H.A.M. and M.M.; Methodology, M.A.H. and G.H.; Project administration, M.A.H. and M.M.M.; Resources, M.A.H. and M.M.M.; Supervision, M.A.H. and M.M.M.; Validation, M.A.H.; Visualization, G.H.; Writing, original draft, G.H., H.S.Y., H.A.M. and M.M.; Writing, review and editing, M.A.H. and M.M.M. All authors have read and agreed to the published version of the manuscript.

Funding: This research was funded by the United Arab Emirates University through the Summer Undergraduate Research Experience (SURE+) program, grant number G00003989.

Data Availability Statement: The data that support the findings of this study are available upon request from the corresponding author.

Conflicts of Interest: The authors declare no conflict of interest.

Appendix A

Table A1. Comparative of precipitation extreme trends using IMERG Final and CHIRPS.

Coordinates		Indices	Trend	
Latitude	**Longitude**		**IMERG**	**CHIRPS**
25.15	56.15	R10	SP	P
		R20	P	P
		R25	NT	P
		CWD	P	SP
		R95	P	P
		PRCPTOT	P	P
25.15	56.25	R10	SP	P
		R20	P	P
		R25	P	P
		CWD	P	P
		R95	P	P
		PRCPTOT	SP	SP
25.25	56.25	R10	SP	P
		R20	P	P
		R25	P	P
		CWD	P	P
		R95	P	P
		PRCPTOT	SP	P
25.25	56.15	R10	SP	SP
		R20	P	P
		R25	P	P
		CWD	P	P
		R95	P	P
		PRCPTOT	P	P
25.55	56.15	R10	P	P
		R20	P	P
		R25	P	P
		CWD	P	P
		R95	P	P
		PRCPTOT	P	P
25.65	56.15	R10	P	P
		R20	P	P
		R25	P	P
		CWD	P	P
		R95	N	P
		PRCPTOT	P	P

Table A1. *Cont.*

Coordinates		Indices	Trend	
Latitude	Longitude		IMERG	CHIRPS
25.65	56.05	R10	P	P
		R20	P	P
		R25	P	P
		CWD	SP	P
		R95	P	P
		PRCPTOT	P	P
25.55	56.05	R10	P	P
		R20	P	P
		R25	P	P
		CWD	SP	P
		R95	P	P
		PRCPTOT	P	P
25.35	56.05	R10	P	P
		R20	P	P
		R25	P	P
		CWD	SP	P
		R95	P	P
		PRCPTOT	P	P

Note: NT = no trend, P = positive trend, SP = significant positive trend, N = negative trend, and SN = significant negative trend.

References

1. Costache, R.; Arabameri, A.; Blaschke, T.; Pham, Q.B.; Pham, B.T.; Pandey, M.; Arora, A.; Linh, N.T.T.; Costache, I. Flash-Flood Potential Mapping Using Deep Learning, Alternating Decision Trees and Data Provided by Remote Sensing Sensors. *Sensors* **2021**, *21*, 280. [CrossRef] [PubMed]
2. Hinge, G.; Hamouda, M.A.; Long, D.; Mohamed, M.M. Hydrologic Utility of Satellite Precipitation Products in Flood Prediction: A Meta-Data Analysis and Lessons Learnt. *J. Hydrol.* **2022**, *612*, 128103. [CrossRef]
3. Fekete, A.; Sandholz, S. Here Comes the Flood, but Not Failure? Lessons to Learn after the Heavy Rain and Pluvial Floods in Germany 2021. *Water* **2021**, *13*, 3016. [CrossRef]
4. Bisht, S.; Chaudhry, S.; Sharma, S.; Soni, S. Assessment of Flash Flood Vulnerability Zonation through Geospatial Technique in High Altitude Himalayan Watershed, Himachal Pradesh India. *Remote Sens. Appl. Soc. Environ.* **2018**, *12*, 35–47. [CrossRef]
5. Yagoub, M.M.; Alsereidi, A.A.; Mohamed, E.A.; Periyasamy, P.; Alameri, R.; Aldarmaki, S.; Alhashmi, Y. Newspapers as a Validation Proxy for GIS Modeling in Fujairah, United Arab Emirates: Identifying Flood-Prone Areas. *Nat. Hazards* **2020**, *104*, 111–141.
6. Ma, M.; Wang, H.; Jia, P.; Tang, G.; Wang, D.; Ma, Z.; Yan, H. Application of the GPM-IMERG Products in Flash Flood Warning: A Case Study in Yunnan, China. *Remote Sens.* **2020**, *12*, 1954. [CrossRef]
7. Zubieta, R.; Getirana, A.; Espinoza, J.C.; Lavado-Casimiro, W.; Aragon, L. Hydrological Modeling of the Peruvian–Ecuadorian Amazon Basin Using GPM-IMERG Satellite-Based Precipitation Dataset. *Hydrol. Earth Syst. Sci.* **2017**, *21*, 3543–3555. [CrossRef]
8. da Amorim, J.S.; Viola, M.R.; Junqueira, R.; de Oliveira, V.A.; Mello, C.R. de Evaluation of Satellite Precipitation Products for Hydrological Modeling in the Brazilian Cerrado Biome. *Water* **2020**, *12*, 2571. [CrossRef]
9. Jiang, L.; Bauer-Gottwein, P. How Do GPM IMERG Precipitation Estimates Perform as Hydrological Model Forcing? Evaluation for 300 Catchments across Mainland China. *J. Hydrol.* **2019**, *572*, 486–500. [CrossRef]
10. Behrangi, A.; Khakbaz, B.; Jaw, T.C.; AghaKouchak, A.; Hsu, K.; Sorooshian, S. Hydrologic Evaluation of Satellite Precipitation Products over a Mid-Size Basin. *J. Hydrol.* **2011**, *397*, 225–237. [CrossRef]
11. Sun, R.; Yuan, H.; Liu, X.; Jiang, X. Evaluation of the Latest Satellite–Gauge Precipitation Products and Their Hydrologic Applications over the Huaihe River Basin. *J. Hydrol.* **2016**, *536*, 302–319.
12. Li, W.; Jiang, Q.; He, X.; Sun, H.; Sun, W.; Scaioni, M.; Chen, S.; Li, X.; Gao, J.; Hong, Y. Effective Multi-Satellite Precipitation Fusion Procedure Conditioned by Gauge Background Fields over the Chinese Mainland. *J. Hydrol.* **2022**, *610*, 127783. [CrossRef]

13. Mahmoud, M.T.; Mohammed, S.A.; Hamouda, M.A.; Mohamed, M.M. Impact of Topography and Rainfall Intensity on the Accuracy of Imerg Precipitation Estimates in an Arid Region. *Remote Sens.* **2021**, *13*, 13. [CrossRef]
14. Mahmoud, M.T.; Hamouda, M.A.; Mohamed, M.M. Spatiotemporal Evaluation of the GPM Satellite Precipitation Products over the United Arab Emirates. *Atmos. Res.* **2019**, *219*, 200–212.
15. Huffman, G.J.; Bolvin, D.T.; Braithwaite, D.; Hsu, K.; Joyce, R.; Xie, P.; Yoo, S.-H. NASA Global Precipitation Measurement (GPM) Integrated Multi-Satellite Retrievals for GPM (IMERG). *Algorithm Theor. Basis Doc. Version* **2015**, *4*, 26.
16. Giannaros, C.; Dafis, S.; Stefanidis, S.; Giannaros, T.M.; Koletsis, I.; Oikonomou, C. Hydrometeorological Analysis of a Flash Flood Event in an Ungauged Mediterranean Watershed under an Operational Forecasting and Monitoring Context. *Meteorol. Appl.* **2022**, *29*, e2079.
17. Ouaba, M.; Saidi, M.E.; Alam, M.J. Bin Flood Modeling through Remote Sensing Datasets Such as LPRM Soil Moisture and GPM-IMERG Precipitation: A Case Study of Ungauged Basins across Morocco. *Earth Sci. Inform.* **2023**, *16*, 653–674.
18. Rachdane, M.; El Khalki, E.M.; Saidi, M.E.; Nehmadou, M.; Ahbari, A.; Tramblay, Y. Comparison of High-Resolution Satellite Precipitation Products in Sub-Saharan Morocco. *Water* **2022**, *14*, 3336.
19. Saouabe, T.; El Khalki, E.M.; Saidi, M.E.M.; Najmi, A.; Hadri, A.; Rachidi, S.; Jadoud, M.; Tramblay, Y. Evaluation of the GPM-IMERG Precipitation Product for Flood Modeling in a Semi-Arid Mountainous Basin in Morocco. *Water* **2020**, *12*, 2516.
20. Downer, C.W.; Ogden, F.L. GSSHA: Model to Simulate Diverse Stream Flow Producing Processes. *J. Hydrol. Eng.* **2004**, *9*, 161–174. [CrossRef]
21. Al-Areeq, A.M.; Al-Zahrani, M.A.; Sharif, H.O. Physically-Based, Distributed Hydrologic Model for Makkah Watershed Using GPM Satellite Rainfall and Ground Rainfall Stations. *Geomat. Nat. Hazards Risk* **2021**, *12*, 1234–1257. [CrossRef]
22. Furl, C.; Ghebreyesus, D.; Sharif, H.O. Assessment of the Performance of Satellite-Based Precipitation Products for Flood Events across Diverse Spatial Scales Using GSSHA Modeling System. *Geosciences* **2018**, *8*, 191. [CrossRef]
23. Sharif, H.O.; Al-Zahrani, M.; Hassan, A. El Physically, Fully-Distributed Hydrologic Simulations Driven by GPM Satellite Rainfall over an Urbanizing Arid Catchment in Saudi Arabia. *Water* **2017**, *9*, 163. [CrossRef]
24. Medina, Y.; Muñoz, E. Analysis of the Relative Importance of Model Parameters in Watersheds with Different Hydrological Regimes. *Water* **2020**, *12*, 2376.
25. Merabtene, T.; Siddique, M.; Shanableh, A. Assessment of Seasonal and Annual Rainfall Trends and Variability in Sharjah City, UAE. *Adv. Meteorol.* **2016**, *2016*, 6206238.
26. Chowdhury, R.; Mohamed, M.M.A.; Murad, A. Variability of Extreme Hydro-Climate Parameters in the North-Eastern Region of United Arab Emirates. *Procedia Eng.* **2016**, *154*, 639–644.
27. Sherif, M.; Akram, S.; Shetty, A. Rainfall Analysis for the Northern Wadis of United Arab Emirates: A Case Study. *J. Hydrol. Eng.* **2009**, *14*, 535–544.
28. Sherif, M.M.; Mohamed, M.M.; Shetty, A.; Almulla, M. Rainfall-Runoff Modeling of Three Wadis in the Northern Area of UAE. *J. Hydrol. Eng.* **2011**, *16*, 10–20. [CrossRef]
29. Sherif, M.M.; Al Mahmoudy, A.; Garamoon, H.; Kasimov, A.; Akram, S.; Ebraheem, A.M.; Shetty, A. Assessment of the Effectiveness of Al Bih, Al Tawiyean and Ham Dams in Groundwater Recharge Using Numerical Models. *Final Rep.* **2005**, *1*.
30. Funk, C.C.; Peterson, P.J.; Landsfeld, M.F.; Pedreros, D.H.; Verdin, J.P.; Rowland, J.D.; Romero, B.E.; Husak, G.J.; Michaelsen, J.C.; Verdin, A.P. A Quasi-Global Precipitation Time Series for Drought Monitoring. *US Geol. Surv. Data Ser.* **2014**, *832*, 1–12.
31. Katsanos, D.; Retalis, A.; Michaelides, S. Validation of a High-Resolution Precipitation Database (CHIRPS) over Cyprus for a 30-Year Period. *Atmos. Res.* **2016**, *169*, 459–464. [CrossRef]
32. Hinge, G.; Mohamed, M.M.; Long, D.; Hamouda, M.A. Meta-Analysis in Using Satellite Precipitation Products for Drought Monitoring: Lessons Learnt and Way Forward. *Remote Sens.* **2021**, *13*, 4353.
33. Hinge, G.; Mazumdar, M.; Deb, S.; Kalita, M.K. District-Level Assessment of Changes in Extreme Rainfall Indices in Barak and Other Basins in Indian Himalayan States: Risks and Opportunities. *Model. Earth Syst. Environ.* **2021**, *8*, 1145–1155.
34. Zhan, Y.-J.; Ren, G.-Y.; Shrestha, A.B.; Rajbhandari, R.; Ren, Y.-Y.; Sanjay, J.; Xu, Y.; Sun, X.-B.; You, Q.-L.; Wang, S. Changes in Extreme Precipitation Events over the Hindu Kush Himalayan Region during 1961–2012. *Adv. Clim. Chang. Res.* **2017**, *8*, 166–175.
35. Zhang, X.; Yang, F. RClimDex (1.0) User Manual. *Clim. Res. Branch Environ. Can.* **2004**, *22*, 13–14.
36. Kendall, M.G. *Rank Correlation Methods*, 4th ed.; Charles Griffin: London, UK, 1975; ISBN 0-85264-199-0.
37. Hamed, K.H.; Rao, A.R. A Modified Mann-Kendall Trend Test for Autocorrelated Data. *J. Hydrol.* **1998**, *204*, 182–196. [CrossRef]
38. Tatalovich, Z.; Wilson, J.P.; Cockburn, M. A Comparison of Thiessen Polygon, Kriging, and Spline Models of Potential UV Exposure. *Cartogr. Geogr. Inf. Sci.* **2006**, *33*, 217–231. [CrossRef]
39. Chen, F.-W.; Liu, C.-W. Estimation of the Spatial Rainfall Distribution Using Inverse Distance Weighting (IDW) in the Middle of Taiwan. *Paddy Water Environ.* **2012**, *10*, 209–222. [CrossRef]
40. Karra, K.; Kontgis, C.; Statman-Weil, Z.; Mazzariello, J.C.; Mathis, M.; Brumby, S.P. Global Land Use/Land Cover with Sentinel 2 and Deep Learning. In Proceedings of the 2021 IEEE International Geoscience and Remote Sensing Symposium IGARSS, Brussels, Belgium, 11–16 July 2021; pp. 4704–4707.
41. Downer, C.W.; Ogden, F.L. Gridded Surface Subsurface Hydrological Analysis (GSSHA) User's Manual; Version 1.43 for Watershed Modeling System 6.1. 2006. Available online: http://wmsdocs.aquaveo.com/gssha_manual_erdc.pdf (accessed on 10 October 2022).

42. Stefanidis, S.; Dafis, S.; Stathis, D. Evaluation of Regional Climate Models (RCMs) Performance in Simulating Seasonal Precipitation over Mountainous Central Pindus (Greece). *Water* **2020**, *12*, 2750.
43. Kazamias, A.-P.; Sapountzis, M.; Lagouvardos, K. Evaluation of GPM-IMERG Rainfall Estimates at Multiple Temporal and Spatial Scales over Greece. *Atmos. Res.* **2022**, *269*, 106014.
44. Saltelli, A. Sensitivity Analysis for Importance Assessment. *Risk Anal.* **2002**, *22*, 579–590. [CrossRef] [PubMed]
45. Saha, G.C.; Li, J.; Thring, R.W. Understanding the Effects of Parameter Uncertainty on Temporal Dynamics of Groundwater-Surface Water Interaction. *Hydrology* **2017**, *4*, 28. [CrossRef]
46. Braud, I.; Roux, H.; Anquetin, S.; Maubourguet, M.-M.; Manus, C.; Viallet, P.; Dartus, D. The Use of Distributed Hydrological Models for the Gard 2002 Flash Flood Event: Analysis of Associated Hydrological Processes. *J. Hydrol.* **2010**, *394*, 162–181. [CrossRef]
47. Ogden, F.L.; Raj Pradhan, N.; Downer, C.W.; Zahner, J.A. Relative Importance of Impervious Area, Drainage Density, Width Function, and Subsurface Storm Drainage on Flood Runoff from an Urbanized Catchment. *Water Resour. Res.* **2011**, *47*. [CrossRef]
48. Fattahi, A.M.; Hosseini, K.; Farzin, S.; Mousavi, S.-F. An Innovative Approach of GSSHA Model in Flood Analysis of Large Watersheds Based on Accuracy of DEM, Size of Grids, and Stream Density. *Appl. Water Sci.* **2023**, *13*, 33. [CrossRef]